Inorganic Chemistry

Article

pubs.acs.org/IC

A Simple Route to Alloyed Quaternary Nanocrystals Ag−In−Zn−S with Shape and Size Control

Grzegorz Gabka,[†] Piotr Bujak,*[,†] Kamila Giedyk,[†] Andrzej Ostrowski,[†] Karolina Malinowska,[‡] Jerzy Herbich,[§] Barbara Golec,[§] Ireneusz Wielgus,[†] and Adam Pron[†]

[†]Faculty of Chemistry, Warsaw University of Technology, Noakowskiego 3, 00-664 Warsaw, Poland

[‡]Faculty of Chemistry, University of Warsaw, Pasteura 1, 02-093 Warsaw, Poland

[§]Institute of Physical Chemistry, Polish Academy of Sciences, Kasprzaka 44/52, 01-224 Warsaw, Poland

Supporting Information

ABSTRACT: A convenient method of the preparation of alloyed quaternary Ag−In−Zn−S nanocrystals is elaborated, in which a multicomponent mixture of simple and commercially available precursors, namely, silver nitrate, indium(III) chloride, zinc stearate, 1-dodecanethiol, and sulfur, is used with 1-octadecene as a solvent. The formation of quaternary nanocrystals necessitates the use of an auxiliary sulfur precursor, namely, elemental sulfur dissolved in oleylamine, in addition to 1-dodecanethiol. Without this additional precursor binary ZnS nanocrystals are formed. The optimum reaction temperature of 180 °C was also established. In these conditions shape, size, and composition of the resulting nanocrystals can be adjusted in a controlled manner by changing the molar ratio of the precursors in the reaction mixture. For low zinc stearate contents anisotropic rodlike (ca.3 nm x 10 nm) and In-rich nanocrystals are obtained. This is caused by a significantly higher reactivity of the indium precursor as compared to the zinc one. With increasing zinc precursor content the reactivities of both precursors become more balanced, and the resulting nanocrystals are smaller (1.5−4.0 nm) and become Zn-rich as evidenced by transmission electron microscopy, X-ray diffraction, and energy-dispersive spectrometry investigations. Simultaneous increases in the zinc and sulfur precursor content result in an enlargement of nanocrystals (2.5 to 5.0 nm) and further increase in the molar ZnS content (up to 0.76). The prepared nanoparticles show stable photoluminescence with the quantum yield up to 37% for In and Zn-rich nanocrystals. Their hydrodynamic diameter in toluene dispersion, determined by dynamic light scattering, is roughly twice larger than the diameter of their inorganic core.

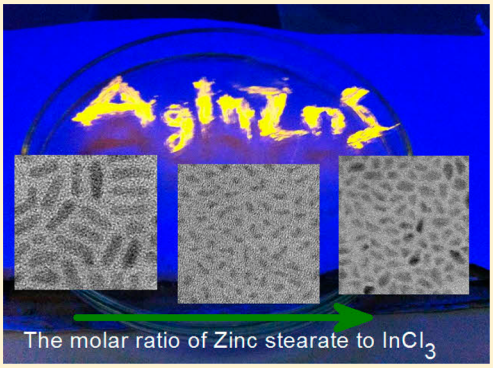

INTRODUCTION

Zero-dimensional[1,2] and one-dimensional[3] colloidal binary semiconductor nanocrystals of controlled size, frequently termed as colloidal quantum dots and quantum rods, respectively, were successfully synthesized more than two decades ago. Since then, considerable research has been carried out on account of their size-dependent electronic and optical properties, which are vital for many applications, such as biomedical fluorophores,[4−7] light-emitting diodes (LEDs),[8−10] and photovoltaic cells (PC),[11,12] to name a few.

Unfortunately, binary compounds showing desired spectroscopic properties frequently contain toxic elements such as Cd, Pb, or Hg. For these reasons heavy metals-free ternary semiconductor nanocrystals were later developed, which could be considered as promising alternatives for the binary compounds. Among them $AgInS_2$, $CuInS_2$, and $CuInSe_2$ are of special interest due to appropriate band-gap energies for bulk materials (e.g., 1.87 eV for orthorhombic $AgInS_2$, 1.53 eV for chalcopyrite $CuInS_2$, 1.05 eV for chalcopyrite $CuInSe_2$).[13] These band gaps can be additionally tuned through the quantum confinement effect. Moreover, the above compounds are direct band-gap semiconductors with correspondingly high optical absorption coefficients.[14] In contrast to other materials considered for applications in thin-film solar cells, such as CdTe or amorphous silicon (a-Si), they are stable under long-term excitation.[15] Alloying Cu−In−S ternary semiconductors with ZnS (whose optical band gap E_g = 3.7 eV) yields nanocrystals with band gaps covering almost the whole visible spectrum as well as a part of the near-infrared (NIR), which is of special interest in both solar energy conversion devices and fluorescence emitters.[16,17] The introduction of zinc in their lattice leads to quaternary systems with high photoluminescence quantum yields (QYs). In 2009 Pan et al.[18] reported the synthesis of quaternary Cu−In−Zn−S nanocrystals showing either cubic or hexagonal structures. The band gaps of these alloyed nanocrystals could be tuned in a broad range from 1.5 to 3.7 eV by changing the ratio of $CuInS_2$ to ZnS. The resulting nanocrystals exhibited photoluminescence QYs up to 70%.[19]

Received: January 8, 2014
Published: May 1, 2014

   dx.doi.org/10.1021/ic500046m | Inorg. Chem. 2014, 53, 5002−5012

Solid solutions were also obtained in the $AgInS_2$–ZnS quaternary system, however, via thermal decomposition of a single diethyldithiocarbamate-type precursor containing all three metals, namely, $(AgIn)_xZn_{2(1-x)}(S_2CN(C_2H_5)_2)_4$, x = 0.4, 0.6, 1.0. The resulting nanocrystals showed the chalcopyrite structure and exhibited photoluminescence QY reaching 24%.[20] Moreover, their emission peak could be controllably shifted from 720 to 540 nm with increasing fraction of ZnS in the solid solution.[20] Very recently Yang et al.[21] prepared $AgInS_2$–ZnS solid solution nanorods (with an average length of ca. 32 nm) by a single-step one-pot solvothermal method, using the same type of precursor as described above. The measured photoluminescence QY was over 32.5%, that is, higher than that reported in the paper of Torminoto et al.[20] for this quaternary system. On the basis of the high-resolution transmission electron microscopy (HRTEM) images and the analysis of single nanorods the authors proposed an anisotropic growth mechanism for these nanoparticles.

Tang et al.[22] prepared $AgInS_2$–ZnS nanoparticles using a hot injection method in which zinc stearate was added to a mixture of indium acetate, silver nitrate, oleic acid, 1-dodecanethiol (DDT), and trioctylphosphine (TOP) in 1-octadecene (ODE). Individual as-prepared nanocrystals showed a two-phase structure of chalcopyrite $AgInS_2$ and cubic ZnS, termed a heterodimer structure. Their emission color could be tuned from red to green by annealing in the temperature range from 90 to 180 °C, through formation of the solid solutions at the interface. Samples annealed at 180 °C showed the highest photoluminescence QY of 38%. More recently, a similar approach was applied to the preparation of photoluminescent Ag–In–Zn–S nanocrystals, in which the solid solution formation was assured through annealing-induced cation diffusion.[23,24] The resulting nanocrystals exhibited photoluminescence QYs of 41% and 32%, respectively. Ag–In–Zn–S nanocrystals were also prepared in aqueous media (mainly for biological use) showing photoluminescence QYs below 30%.[25]

This brief literature search clearly indicates that all successful attempts of the preparation of alloyed $AgInS_2$–ZnS nanocrystals involved the use of a rather sophisticated, tailor-made one-component precursor, the use of multicomponent precursors was very scarce,[26] and frequently required *post*reaction processing, which involved cation exchange.[22−24] In this work, we report the synthesis of quaternary Ag–In–Zn–S nanocrystals with different shapes, sizes, and compositions using the simple and commercially available chemicals silver nitrate, indium(III) chloride, zinc stearate, and DDT as precursors and ODE as solvent. The use of DDT without the admixture of an additional ligand source, such as oleic acid, for example, enabled the preparation of nanocrystals whose sizes, shapes, and compositions could be easily controlled by the ratio of the precursors. The off-stoichiometry effects on crystal structure and optical properties of the quaternary Ag–In–Zn–S system were also observed and discussed. The proposed simple and very versatile preparation strategy consists of one step, in contrast to the already the reported two-step procedures for similar nanocrystals.[27] Moreover, it enables the synthesis of $AgInS_2$–ZnS alloyed nanocrystals in the composition range from 0.24 mol % of $AgInS_2$ to 0.75 mol % of $AgInS_2$.

EXPERIMENTAL SECTION

Materials. Silver nitrate (99%), indium(III) chloride (98%), zinc stearate (technical grade), 1-dodecanethiol (DDT, 98%), sulfur (99%), 1-octadecene (ODE, 90%), and oleylamine (OA, 70%) were supplied by Sigma-Aldrich.

Preparation of Ag–In–Zn–S Nanocrystals. In a typical process, silver nitrate (0.03 g, 0.17 mmol), indium(III) chloride (0.132 g, 0.59 mmol), zinc stearate (0.63 g, 1.0 mmol), and DDT (0.4 g, 0.98 mmol) were mixed with ODE (15 mL) in a three-neck flask. The mixture was heated under argon flow to 150 °C until a homogeneous solution was formed. Then sulfur (15 mg, 0.47 mmol) dissolved in 1 mL of OA was quickly injected into the reaction solution. The temperature was raised to 180 °C, and the mixture was kept at this temperature for 60 min. Upon heating, the color changed rapidly from yellow through red and finally to black. After the mixture was cooled to room temperature, toluene (20 mL) was added, and the reaction mixture was centrifuged—the isolated black precipitate was separated. The supernatant was treated with 30 mL of acetone leading to the precipitation of the desired fraction of nanocrystals. The nanocrystals were separated by centrifugation (7000 rpm, 5 min) and then redispersed in toluene (or chloroform).

Characterization. X-ray diffraction patterns were recorded on a Seifert HZG-4 automated diffractometer using Cu $K\alpha_{1,2}$ radiation (1.5418 Å). The data were collected in the Brag-Brentano ($\theta/2\theta$) horizontal geometry (flat reflection mode) between 10 and 70° (2θ) in 0.04° steps, at 10 s step^{-1}. The optics of the HZG–4 diffractometer was a system of primary Soller slits between the X–ray tube and the fixed aperture slit of 2.0 mm. One scattered–radiation slit of 2 mm was placed after the sample, followed by the detector slit of 0.2 mm. The X-ray tube operated at 40 kV and 40 mA. TEM analyses were performed on Zeiss Libra 120 electron microscope operating at 120 kV. Elemental compositions of the prepared nanocrystals were determined by energy-dispersive spectroscopy (EDS). Absorption spectra were run on a Shimadzu UV-2700 spectrophotometer. Steady-state fluorescence was recorded using Edinburgh FS 900 CDT fluorometer (Edinburgh Analytical Instruments). Emission QYs were measured using quinine sulfate in 0.05 mol dm^{-3} H_2SO_4 (φ_{fl} = 0.51) as a standard.[28] ^{1}H NMR spectra were recorded on a Varian Mercury (400 MHz) spectrometer and referenced with respect to tetramethylsilane and solvents. The hydrodynamic diameters were measured by dynamic light scattering (DLS) using Zetasizer Nano ZS (ZEN3600, Malvern Instruments) with a laser illumination at 633 nm.

RESULTS AND DISCUSSION

The main issue in the preparation of homogeneously alloyed ternary or quaternary nanocrystals from a multicomponent mixture of precursors is a proper balance of reactivities of the two (or three) cationic precursors, which in principle can be done by the proper selection of reactivity modulating ligands, the solvent matrix composition, and the reaction temperature. This approach was successfully applied in the preparation of Cu–In–Zn–S nanocrystals by Zhang et al.[19] Inspired by this work we have elaborated a modified heating-up method of alloyed nanocrystals preparation in the Ag–In–Zn–S quaternary system. In this procedure silver nitrate, indium(III) chloride, and zinc stearate were used as precursors of the cations, together with DDT (ligand and sulfur source), sulfur, and ODE as a solvent. Alloyed nanocrystals of different compositions were obtained by varying In/Zn and Zn/S (zinc stearate/DDT) molar ratios.

In the subsequent part of the paper we consecutively discuss the role of all anionic and cationic precursors of nanocrystals. Several papers describing the preparation of quaternary Cu–In–Zn–S report the use of a small amount of sulfur as an auxiliary precursor in addition to DDT.[18,19] Cold solution of this precursor in OA is usually injected into previously heated

dx.doi.org/10.1021/ic500046m | Inorg. Chem. 2014, 53, 5002−5012

reaction mixture.[29−31] To identify the role of this auxiliary precursor we have performed two sets of Ag−In−Zn−S nanocrystals preparations: with and without injection of the sulfur solution. In each case the molar ratio of other precursors was kept constant: Ag/In/Zn/DDT = 1.0/3.4/8.0/5.6. In the course of the reaction ultraviolet−visible (UV−vis) spectra were periodically measured for solutions obtained by diluting with chloroform small aliquots taken from the reaction mixture. Injection of this precursor solution induced a profound change in the UV−vis spectrum and gave rise to orange photoluminescence, clearly seen upon excitation with a 365 nm UV lamp (see Figures S1 and S2 in Supporting Information). No significant spectral changes could be observed upon further heating of the reaction mixture at 180 °C as well as in the spectra of isolated nanocrystals, redispersed in $CHCl_3$.

If the nanocrystals' preparation reaction was carried out in the same conditions, however, without injection of sulfur in OA a new peak appeared in the UV−vis spectrum at ca. 300 nm, whose intensity increased with the reaction time (see Figure S3 in Supporting Information). No orange photoluminescence was observed; instead, weak blue luminescence could be detected (Figure S4 in Supporting Information). Two fractions of nanocrystals, isolated from the reaction mixture, yielded in their UV−vis spectra clear peaks at 345 and 340 nm, respectively, characteristic of ZnS nanocrystals differing in size.[32]

The obtained results unequivocally show that in the preparation of quaternary Ag−In−Zn−S nanocrystals the injection of the auxiliary sulfur precursor plays a crucial role, facilitating their nucleation and growth.[33,34] In this context investigations of Thomson et al.[35] concerning the reactions of sulfur in the reaction medium should be mentioned. Dissolving sulfur in OA at room temperature produces alkylammonium polysulfides, which decompose when injected into the hot reaction mixture, yielding H_2S whose presence is necessary for the formation of sulfides. At 150 °C complexes of Ag(I) and In(III) with DDT are present in the reaction mixture, which in the absence of the auxiliary sulfur precursor decompose to silver.[36] If no sulfur is added to the reaction mixture used for the preparation of quaternary Ag−In−Zn−S nanocrystals, zinc stearate reacts with DDT (which slowly decomposes with increasing temperature) yielding ZnS nanocrystals.

It is known that indium-rich quaternary nanocrystals of high photoluminescence QY are usually obtained by using high molar ratios of In precursors to Ag precursors.[37−39] We demonstrate here that photoluminescent nanocrystals of controlled composition, size, and shape can be obtained from reaction mixtures of fixed high ratio of Ag/In/DDT = 1.0/3.4/5.6 by varying the content of the Zn precursor. In the applied preparation conditions, independently of the zinc precursor content, side products in a form of a black precipitate are isolated by centrifugation. Nanocrystals remaining in the supernatant are precipitated in the next step by the addition of acetone (see Experimental Section). X-ray diffraction studies of the collected black precipitate indicate a poorly defined product with a few rather broad reflections, which cannot be indexed as originating from possible binary or ternary phases such as $AgInS_2$, ZnS, In_2S_3, and Ag_2S or from their mixture (see Figure S5 in Supporting Information). ^1H NMR spectra of these side products show the presence of DDT and ODE, the latter being used as a solvent in the reaction medium. No signals attributable to stearic acid could be detected (Supporting Information, Figure S6).

Diffractograms of nanocrystals precipitated with acetone from the supernatant are presented in Figure 1. In each

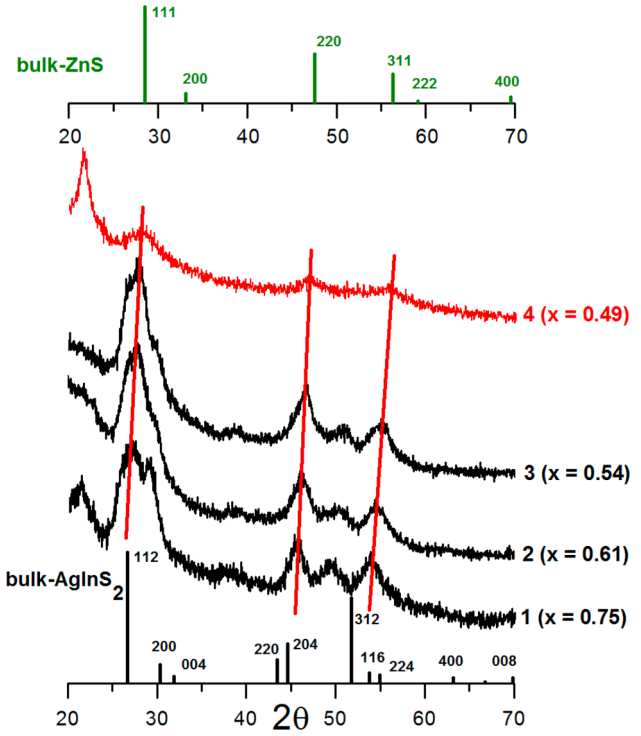

Figure 1. X-ray diffractograms of alloyed Ag−In−Zn−S quaternary nanocrystals obtained from reaction mixtures of fixed Ag/In/DDT ratio = 1.0/3.4/5.6 and varying Ag/Zn ratio: 1:3.6 (batch **1**); 1:5.6 (batch **2**); 1:7.2 (batch **3**), and 1:8.0 (batch **4**). The molar fraction of $AgInS_2$ in these nanocrystals, *x*, is indicated next to each diffractogram.

diffractogram, in the 2θ range from 25° to 70°, three broad reflections can be seen at positions intermediate between the positions of (112), (204), (312) reflections of tetragonal $AgInS_2$[40] and the positions of (111), (220), (311) reflections of cubic ZnS.[41] This can be considered as a strong indication of alloying since a mixture of pure $AgInS_2$ and ZnS phases would result in a superposition of the corresponding diffractograms with the position of particular reflections being unchanged. Using Vegard's law, which predicts a linear relationship between the crystallographic cell parameters and the composition of the alloyed crystal, it is possible to determine the molar fraction of $AgInS_2$ in the quaternary $AgInS_2$−ZnS nanocrystals studied in this research using eq 1:

$$c_x = c^{ZnS} + (c^{AgInS_2} - c^{ZnS})x \quad (1)$$

where c_x is the position of a given reflection, c^{ZnS} and c^{AgInS_2} relate the positions of the corresponding reflections in pure ZnS and pure $AgInS_2$, and *x* is a molar fraction of $AgInS_2$ in the alloyed compound. The values of *x* obtained for nanocrystals prepared from reaction mixtures of increasing Zn precursor contents are indicated in Figure 1, next to the diffractograms.

As expected, the molar fraction of $AgInS_2$ in the resulting quaternary nanocrystals decreases with increasing Zn/In ratios. As evidenced by their TEM images (Figure 2) and by their histograms (Figure S7 of Supporting Information) the nanocrystals' size and shape change with their composition. Nanocrystals from batch **1** ($x_{AgInS_2} = 0.75$) are relatively large (8 nm) and ellipsoid in shape, with an average aspect ratio of 1.5.

dx.doi.org/10.1021/ic500046m | Inorg. Chem. 2014, 53, 5002−5012

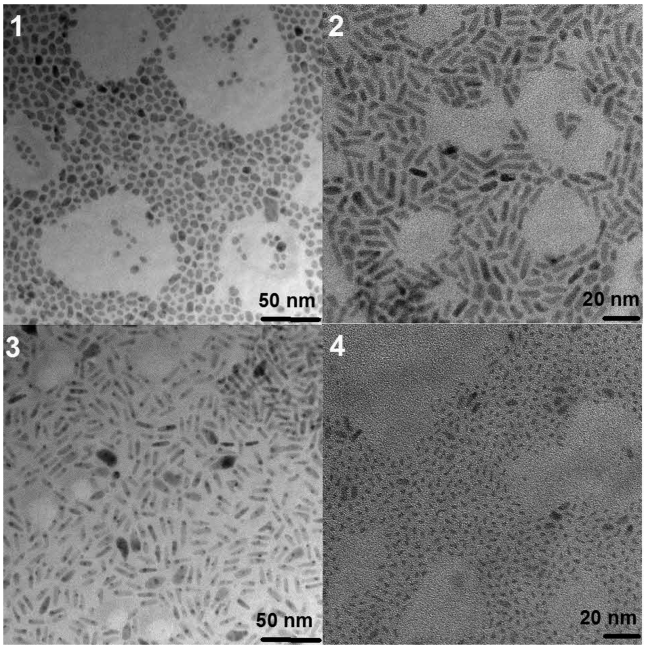

Figure 2. TEM images of nanocrystals of batches **1**, **2**, **3**, and **4**.

With decreasing x (batches **2** (x_{AgInS_2} = 0.61) and **3** (x_{AgInS_2} = 0.54) the nanocrystals adopt a rodlike morphology, and their aspect ratio increases to 3.5 and 4.2, respectively. Note that the observed increase of the aspect ratio is not caused by an increase of the nanocrystals length but by a decrease in their width. Nanocrystals from batch **4** (x_{AgInS_2} = 0.49) are small (2.5 nm) and cubic or rodlike in shape.

Differences in the sizes and shapes of nanocrystals of batches **1** to **4** originate from the differences between reactivities of Ag, In, and Zn precursors with DDT. It is known that DDT easily forms a polymeric-type complex with silver and indium ions, which facilitates the formation of ternary nanocrystals. The formation of such complexes in the process of tetragonal $AgInS_2$ nanocrystals preparation has previously been reported.[42] In these conditions the reaction of zinc precursor (zinc stearate) with thiol is somehow impeded since the latter has been largely consumed in the formation of the polymeric complex. The alloyed quaternary nanocrystals are therefore formed through an exchange of indium and silver cations for zinc ones. In the case of batch **1** this process favors the formation of large nanocrystals since the conversion of the zinc precursor is slow, and by consequence the supply of stearate capping ligands is also slow. An increase in the zinc precursor concentration in batch **2** leads to its more efficient conversion. As a result the concentration of the stearate surfacial ligands increases in the vicinity of the growing nanocrystal, preventing it from further growth. Note that low-dimensional character of the preformed Ag−In−thiol complex facilitates the growth of anisotropic rod-shaped nanocrystals. This effect is even more pronounced in nanocrystals of batch **3**. In batch **4** the highest degree of the zinc precursor conversion leads to higher content of the stearate surfacial ligands whose presence efficiently inhibits further growth of nanocrystals. The resulting cubic or *quasi*-spherical nanocrystals do not exceed 2.5 nm in size. Close inspection of Figure 2 reveals the presence of a very small fraction of rod-shaped nanocrystals originating from the polymeric complex form. It should be clearly stated that the presence of this complex must be treated as a plausible hypothesis based on previous results obtained for similar systems[42] and in line with the experimental findings reported here.

The diffractograms of batches **4**, **5**, and **6** are shown in Figure 3. Simultaneous increase of the zinc and sulfur precursors

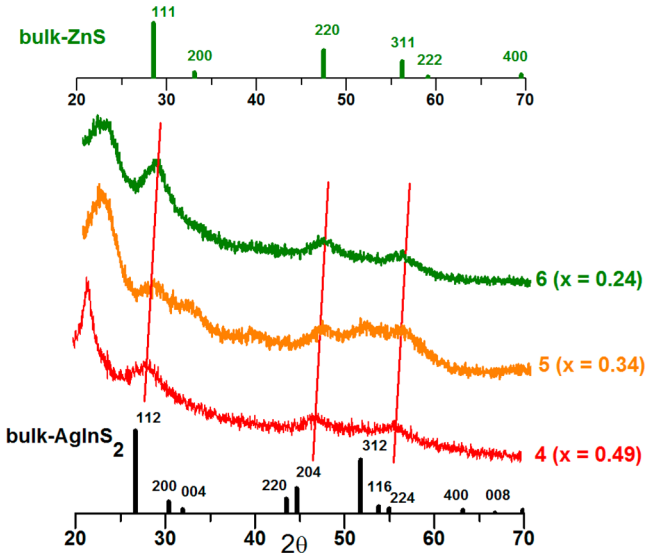

Figure 3. X-ray diffractograms of alloyed Ag−In−Zn−S quaternary nanocrystals obtained from reaction mixtures of Ag/In/Zn/DDT ratio = 1.0/3.4/8.0/5.6 (batch **4**); 1.0/3.4/10.8/11.2 (batch **5**), and 1.0/3.4/13.4/16.8 (batch **6**). The molar fraction of $AgInS_2$ in these nanocrystals, *x*, is indicated next to each diffractogram.

content (batch **5** in Figure 4) leads to quasi-monodispersed nanocrystals of roughly the same size as in batch **4** (see Figure 4), but with a molar fraction of x_{AgInS_2} decreased to 0.34. Further increase of the Zn precursor content and application of an excess of DDT (with respect to the stoichiometric amount) results in the lowest value of x_{AgInS_2} (0.24) and an increase of the nanocrystals size by 1 nm (compare TEM images of batch **5** and **6** in Figure 4). Complete characterization data for the most representative nanocrystals are collected in Table 1.

EDS data corroborate the above-discussed results (see Figure 5 and Table 1). First, the values of x_{AgInS_2} calculated from In and Zn contents reasonably agree with those derived from the X-ray diffractograms being, however, systematically slightly higher. Second, the analytical data clearly confirm higher reactivity of indium precursor with respect to the zinc one since the In/Zn ratio in the nanocrystals is in all cases higher than the corresponding ratio in the reaction mixture. This difference in reactivity can be, however, conveniently modulated by an increase in the content of zinc precursor (zinc stearate) and sulfur precursor (DDT). In Figure 6 the In/Zn ratio in the reaction mixture is plotted versus the analogous ratio in the obtained nanocrystals. It is clear that with increasing content of zinc stearate the difference in the reactivities between indium and zinc precursors steeply decreases. Higher reactivity of indium and, by consequence, higher rate of $AgInS_2$ formation with respect to that of ZnS was previously reported for Ag−In−Zn−S quaternary nanocrystals prepared by thermal decomposition of a single, multifunctional precursor.[21]

The elaborated method of alloyed quaternary Ag−In−Zn−S nanocrystal preparation enables facile control of their size and shape by exploiting differences in the rate of the Ag−S, In−S,

dx.doi.org/10.1021/ic500046m | Inorg. Chem. 2014, 53, 5002−5012

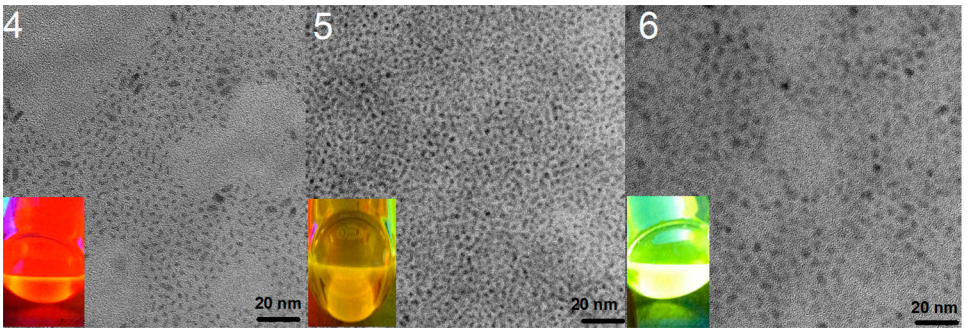

Figure 4. TEM images of nanocrystals of batches **4**, **5**, and **6**.

Table 1. Characteristics of Alloyed Ag−In−Zn−S Quaternary Nanocrystals Prepared Using Different Precursor Ratios

	Ag/In/Zn/DDT[a]	Ag/In/Zn[b]	x_{AgInS_2}[c]	x_{In}[d]	E_g (eV)[e] calc.	E_g (eV)[f] UV	size (nm)[g]	PL (nm)[h]	QY (%)[i]
2	1.0/3.4/5.6/5.6	1.0/15.6/7.6	0.61	0.67	2.53	2.52	2.0−5.0	687	11.2
4	1.0/3.4/8.0/5.6	1.0/11.4/9.5	0.49	0.54	2.75	2.73	1.5−4.0	665	10.2
5	1.0/3.4/10.8/11.2	1.0/5.3/9.9	0.34	0.35	3.03	3.09	1.5−4.0	586	14.3
6	1.0/3.4/13.4/16.8	1.0/5.7/17.5	0.24	0.25	3.22	3.26	2.5−4.5	553	16.5

[a]Precursors molar ratio. [b]Ratio of elements in the nanocrystals from EDS. [c]$AgInS_2$ content from X-ray diffraction. [d]Indium molar content from EDS. [e]Calculated following the formula $E_g(x) = xE_g^{AgInS_2} + (1-x)E_g^{ZnS} - bx(1-x)$, coefficient b taken from ref 43. [f]Optical band gap. [g]Size determined from TEM, in the case of rodlike nanocrystals of batch a this value refers to their diameter, the length is in the range of 6−15 nm. [h]Maximum of the photoluminescence band. [i]Photoluminescence quantum yield.

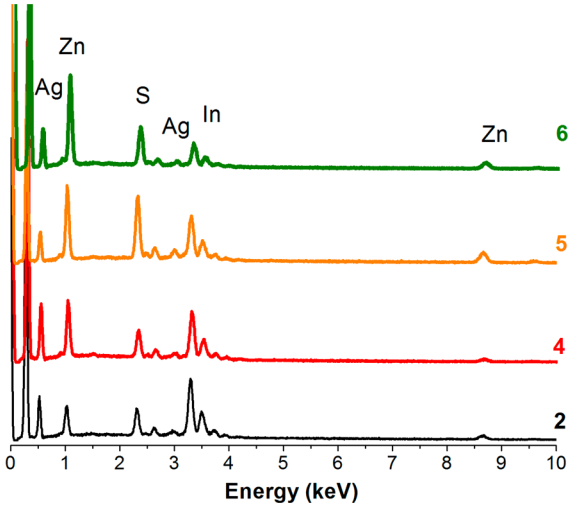

Figure 5. Energy-dispersive spectra of nanocrystals of batches **2**, **4**, **5**, and **6**.

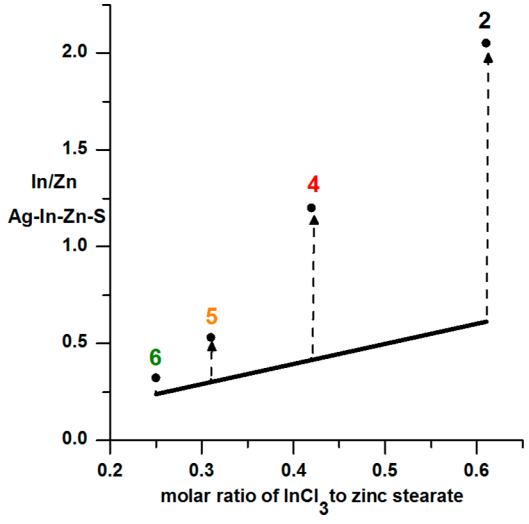

Figure 6. In/Zn ratio in the reaction mixture versus the same ratio in the resulting Ag−In−Zn−S.

and Zn−S bond formation. Depending on the precursor molar ratios in the reaction mixture two mechanisms of nanocrystals formation can be postulated. In the case of lower zinc stearate and DDT content, the nanocrystals are formed via intermediate, polymeric-type complex of silver and indium with thiol (*vide supra*). In these conditions larger, anisotropic nanoparticles are obtained.

With increasing zinc precursor content in the reaction mixture, while keeping the DDT content constant, the size of the nanocrystals diminishes, and at the same time they become spherical. Above a certain content of zinc stearate and DDT no intermediate polymeric complex of silver and indium is formed, and the rate of the bond formation between the three cations and sulfur becomes similar. This is evidenced by the EDS investigations of the prepared nanocrystal composition. Smaller nanocrystals are obtained for more balanced Ag−S, In−S, and Zn−S bond-formation rates. Further increase in the Zn stearate and DDT content in the reaction mixture results in an increase of the nanocrystals' size, which is associated with higher zinc precursor conversion rates.

All the above-discussed preparations of nanocrystals were carried out in the same temperature regime, that is, after injection of the solution of sulfur in OA at 150 °C, the reaction mixture was heated to 180 °C and kept at this temperature for 1 h. Temperature constitutes, however, an additional tool suitable for controlling the nanocrystals' composition, size, and shape. To test the effect of temperature we performed three preparations at three different temperatures (150, 180, and 200 °C) using the same molar ratios of precursors—Ag/In/Zn/DDT = 1.0/3.4/10.8/11.2. The sulfur injection temperature (150 °C) and the reaction time (1 h) were the same as in all previously described cases. Two clear trends could be observed

dx.doi.org/10.1021/ic500046m | *Inorg. Chem.* 2014, 53, 5002−5012

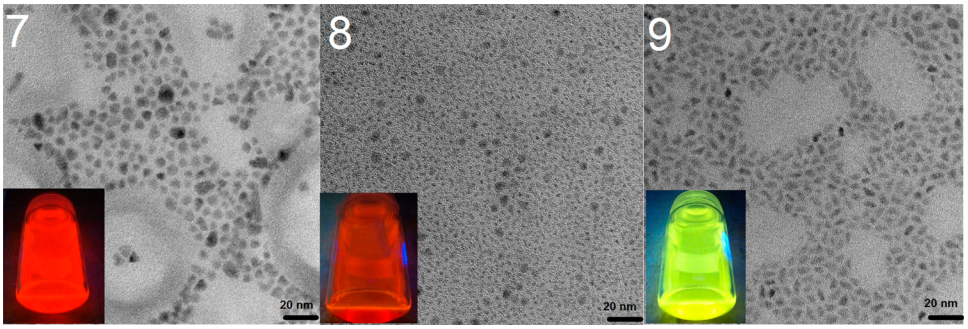

Figure 7. TEM images of nanocrystals of batches 7 (molar ratios of precursors: Ag/In/Zn/DDT = 1/5/4/8); **8** (1/5/6/8); **9** (1/5/20/25).

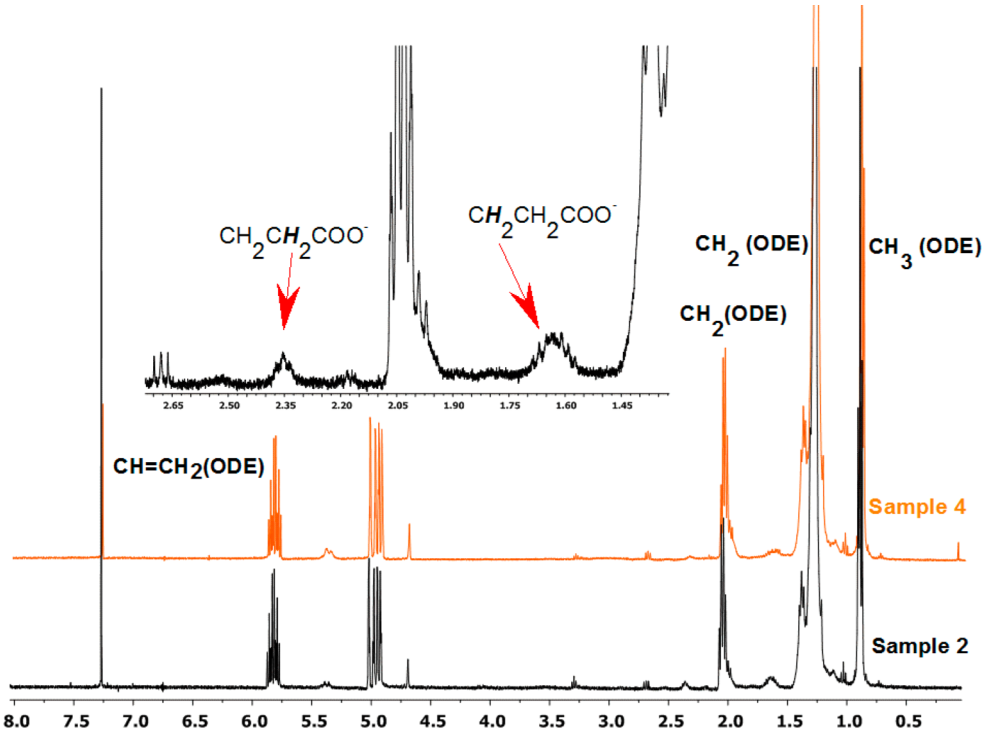

Figure 8. ^{1}H NMR spectra of nanocrystals batches **2** and **4** dispersed in $CDCl_3$.

with increasing reaction temperature: (i) increase of the average nanocrystal size and (ii) increase of the content of zinc in the resulting nanocrystals. In the diffractograms of nanocrystals prepared at 150 and 180 °C adequate Bragg reflections were hardly distinguishable; with increasing reaction temperature they shifted toward the position characteristic of ZnS, indicating increasing content of Zn in the obtained quaternary nanocrystals (see Figure S8 in Supporting Information). This shift was accompanied by a significant decrease of the full width at half-maximum (fwhm) values of the registered Bragg reflections (see Figure S8 in Supporting Information). The enrichment in Zn with increasing temperature was corroborated by the EDS studies, which showed a decrease of the In/Zn ratio from 1/1 in the nanocrystals prepared at 150 °C to 1/2.8 in those synthesized at 200 °C (see Figure S9 in Supporting Information for the complete set of the EDS data). These results confirm findings discussed above that the quaternary nanocrystals growth is limited by the diffusion of zinc precursor to the germs formed from Ag−In−DDT complex. Moreover, they indicate that the temperature of 180 °C is the most appropriate as far as the control of nanocrystals composition and size is concerned.

To verify whether the above outlined picture is valid and whether we properly identified all crucial parameters determining the composition and size of quaternary Ag−In−Zn−S nanocrystals, we prepared three batches of nanocrystals (**7**, **8**, and **9**) in which the ratio of silver to indium precursors was kept constant and equal to 1/5.0, whereas the content of zinc stearate and DDT was changed in a similar manner as in the case of the **1**−**6** series. The molar ratios of the precursors (Ag/In/Zn/DDT) in the reaction medium were as follows: 1/5/4/8 (batch **7**), 1/5/6/8 (batch **8**), 1/5/20/25 (batch **9**). The same trend as in the case of the **1**−**6** series is reproduced (compare Figures 2, 4, and 7). Nanocrystals of larger size (6−8 nm) are obtained for a small content of zinc stearate, its increase leads to the diminishing of the nanoparticle size. Note that in nanocrystals of batch **8** two fractions can be distinguished: the predominant fraction of very small nanocrystals (2−3 nm) and a minority fraction of larger nanocrystals (4−6 nm). Further simultaneous increase in the zinc stearate and DDT content results in an increase of the nanocrystal size to 5−8 nm. One can therefore postulate the same growth mechanism for both series **1**−**6** and **7**−**9**.

dx.doi.org/10.1021/ic500046m | *Inorg. Chem.* 2014, 53, 5002−5012

Complete characterization of the obtained nanocrystals requires the characterization of the initial capping ligands, that is, ligands originating from the reaction medium. ^{1}H NMR is very well-suited for this purpose. In Figure 8 the spectra of two nanocrystals batches (**2** and **4**), dispersed in $CDCl_3$, are compared. No particular differences between the spectra can be noticed, suggesting the same nature of the capping ligands for different compositions of the alloyed Ag−In−Zn−S quaternary nanocrystals. In particular, multiplets characteristic of olefinic protons can be distinguished at 4.9 and 5.9 ppm, corresponding to three protons in the vinyl group (−CH=CH_2) of ODE. Aliphatic protons give rise to (i) a broadened triplet in the range of 0.85−0.95 ppm ascribed to the methyl, $-CH_3$, group; (ii) a strong multiplet in the range of 1.2−1.5 ppm corresponding to the methylene, $-CH_2-$, groups; and (iii) a multiplet at 1.95−2.10 ppm attributed to the methylene group adjacent to the vinyl group. Thus, ODE seems to be the dominant capping ligand in the studied nanocrystals. However, lines of much lower intensity, which cannot be attributed to ODE, can also be seen in the spectra. They are much better distinguishable in the inset of Figure 8. The other possible ligands of the obtained nanocrystals are stearate anion and DDT. Their NMR spectra are very similar, the only disparity being different chemical shifts of the signals originating from α-CH_2- and β-CH_2- groups. In the case of DDT the multiplet corresponding to the methylene group connected to −SH is located in the 2.48−2.55 ppm range, whereas that originating from β-CH_2- appears in the range of 1.20−1.60 ppm.[44] In the spectrum of stearic acid, α-CH_2- protons give rise to a triplet at 2.35 ppm, whereas protons of β-CH_2- give rise to a triplet at 1.63 ppm.[45] The presence of a broadened triplet at 2.35 ppm, together with a multiplet in the range of 1.55−1.70 ppm, unequivocally prove the presence of stearate ligand on the surface of nanocrystals. No spectroscopic indication of the presence of DDT can be found. Thus, the analysis of the NMR spectra suggests the presence of two types of ligands—ODE (which is dominant) and stearic acid. Lines characteristic of DDT are found only in the side product, whose spectrum is shown in Figure S6 of Supporting Information.

To complete the characterization of the nanocrystal−ligand systems we carried out the determination of their hydrodynamic radius using DLS. The hydrodynamic radius describes the effective radius of a nanocrystal, which includes the inorganic core and all ligands coordinated to it. In Figure 9 a histogram of the hydrodynamic diameters determined for nanocrystals of **5** dispersed in toluene is presented as an example.

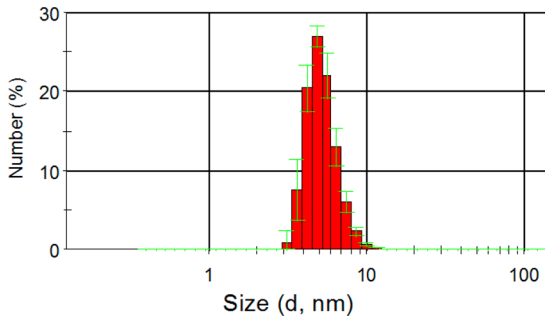

Figure 9. Histogram of hydrodynamic diameters (derived from DLS studies) of nanocrystals dispersed in toluene (batch **5**).

The obtained results are very consistent with TEM image. In this image these spherical nanocrystals are of 2−3.5 nm size (Figure S7 in Supporting Information). Their hydrodynamic diameter varies from 4 to 8 nm. This difference can be ascribed to the presence of the coordinating ligands as well as some solvent molecules constituting additional components of the coordination sphere. The effect of the type of capping ligands on the nanocrystal hydrodynamic radius was previously studied for CdSe/ZnS core−shell nanocrystals capped with trioctylphosphine/trioctylphosphine oxide (TOP/TOPO) ligands and dispersed in the same solvent (toluene).[46] The following correlation was found: $R_H = R_{CdSe} + 2.7$ nm. For the same nanocrystals capped with 6,8-dimercaptooctanoic acid and dispersed in water a different correlation was found: $R_H = 2.2R_{CdSe} + 3.2$ nm.[46] For spherical quaternary nanocrystals investigated in this research (~2.5 nm) the hydrodynamic radius (R_H) was roughly twice bigger than the nanocrystal size as determined by TEM. This rather large value of the hydrodynamic radii measured for the studied quaternary nanocrystals requires some comment. They significantly differ from those found in purely organic macromolecular materials where the predicted ratio of R_H to the gyration radius is ca. 0.67.[47] There are, however, profound differences between these two types of materials. In polymeric materials solvent penetrates random coils, which diffuse in the solution. Nanocrystals consist of a hard inorganic core that is not penetrable for solvent molecules and organic surfacial ligands that, to a first approximation, behave like polymers with respect to solvent molecule penetration. Moreover this surfacial coordination sphere is large and complex because it consists of ligands directly bound to the surface and additional ligands that, although stabilizing the colloidal dispersion, do not form direct bonds with surfacial atoms. In the case of ternary Ag−In−Zn−S nanocrystals ODE belongs to this type of ligand, and its presence is evidenced in the registered ^{1}H NMR spectrum of the prepared nanocrystals (see Figure 8). Coordination spheres of other nanocrystals also contain large amounts of ODE in addition to other types of ligands as reported for example for InP nanocrystals.[48−50] Thus, large values of R_H as compared to the size of nanocrystals obtained from TEM images have their origin in the contribution of the organic coordination sphere to the DLS measurements.

As evidenced from the images presented in Figures 2 and 7, as well as from the data collected in Table 1, the elaborated method of quaternary Ag−In−Zn−S nanocrystals preparation enables facile control of their shape, size, and composition. As a consequence, their optical properties can be precisely tuned. With increasing Zn content their color changes from red to green (see Figure S10 in Supporting Information).

The optical band gap, E_g, of the studied nanocrystals can be conveniently determined from the UV−vis spectra obtained for their dispersions in an appropriate solvent. In this case the $(Ah\nu)^2$ versus $h\nu$ relationship is used, where A = absorbance and $h\nu$ = energy expressed in eV. These plots for nanocrystals of batches **2**, **4**, **5**, and **6** are presented in Figure 10, whereas the obtained E_g values are collected in Table 1. It is clear that E_g increases with the rising Zn content.

For alloyed nanocrystals of a given composition it is possible to calculate the band gap using the E_g values determined for pure components and knowing a molar fraction x.[43,51,52] This is based on the fact that, independently of the nanocrystal size, their E_g versus x relationship reproduces in its character the one obtained for bulk materials.[53] Such calculations have previously

dx.doi.org/10.1021/ic500046m | Inorg. Chem. 2014, 53, 5002−5012

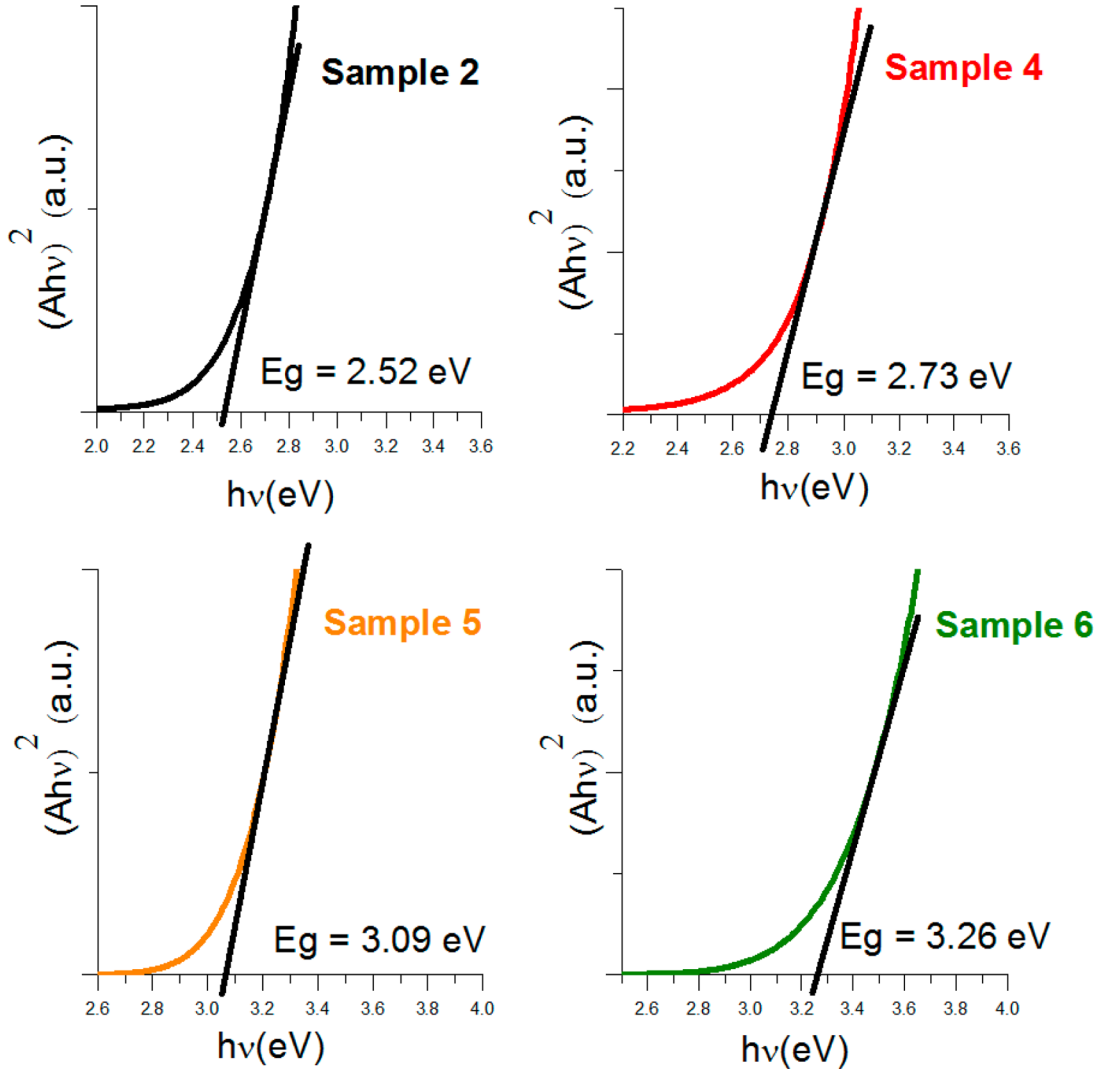

Figure 10. $(Ah\nu)^2$ vs $h\nu$ plots obtained from the UV−vis spectral data of nanocrystals of increasing Zn contents. Toluene dispersions of batches **2**, **4**, **5**, and **6**.

been carried out for alloyed Cu−In−Zn−S nanocrystals.[18,54] In our calculations of E_g we used eq 2[43]

$$E_g(x) = xE_g^{AgInS_2} + (1 - x)E_g^{ZnS} - bx(1 - x) \quad (2)$$

where $E_g^{AgInS_2}$ and E_g^{ZnS} are band gaps of $AgInS_2$ (1.87 eV) and ZnS (3.7 eV),[18,55] x is the molar fraction of $AgInS_2$ in a given alloyed nanocrystal, taken in our case from the X-ray data, and b is a constant (0.2, as in ref 43). The results of theses calculations are collected in Table 1.

The band gaps of the nanocrystals, calculated on the basis of their composition, very well agree with those obtained from the spectroscopic studies. The obtained results clearly indicate that the band gap is predominantly determined by the content of zinc. It is difficult to determine the effect of the nanocrystal size on E_g since the obtained Zn-rich and In-rich nanocrystals differ in size. The quantum confinement effect is dependent on the exciton Bohr radius. This parameter is much higher for $AgInS_2$ (5.5 nm) than it is for ZnS (2.5 nm).[56] Thus, the effect of the size on the optical properties should be more easily observed in In-rich nanocrystals than in Zn-rich ones. In reality this effect is totally obscured in both cases by a very pronounced sensitivity of the nanocrystals' optical and photoluminescence properties to the content of Zn. Therefore, good agreement between the optical and calculated E_g values could be obtained for the same value of constant b in eq 2, despite the fact that this constant should be size-dependent. Anyhow, the contribution of this term of eq 2 is small and accounts for ca. 0.5% of the E_g value in Zn-rich samples and ca. 1.0% for In-rich ones.

An interesting feature of the studied nanocrystals is their tunable, composition-dependent photoluminescence (see Figures 4 and 7 and Figure S10 in Supporting Information). In Figure 11 absorption and emission spectra of the dispersion of nanocrystals of batch **2** in toluene are shown as a representative example.

The observed spectral features are characteristic of the studied family of quaternary nanocrystals. In the absorption spectrum a steep increase of absorbance, extending toward the UV part of the spectrum, is observed. The photoluminescence band is located in the visible region with a large Stokes shift of ca.100 nm and a relatively large fwhm value.[17] Mechanistic studies indicate that the photoluminescence of high QY, observed in alloyed Ag−In−Zn−S nanocrystals, does not originate from an exciton recombination but rather involves recombination of electrons and holes via donor- and acceptor-

dx.doi.org/10.1021/ic500046m | Inorg. Chem. 2014, 53, 5002−5012

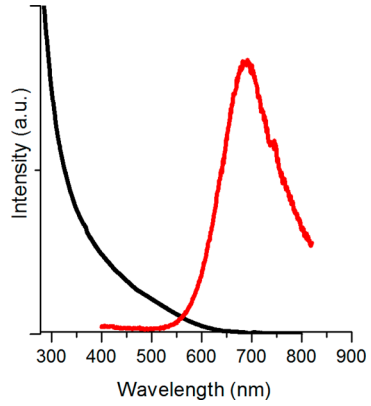

Figure 11. Absorption and emission spectrum of batch **2** nanocrystals dispersion in toluene; λ_{exc} = 375 nm.

type defects present either in the bulk of the nanocrystal or on its surface.[57−61]

In Figure 12a photoluminescence spectra of nanocrystals of batches **2**, **4**, **5**, and **6** are compared. Their hypsochromic shift

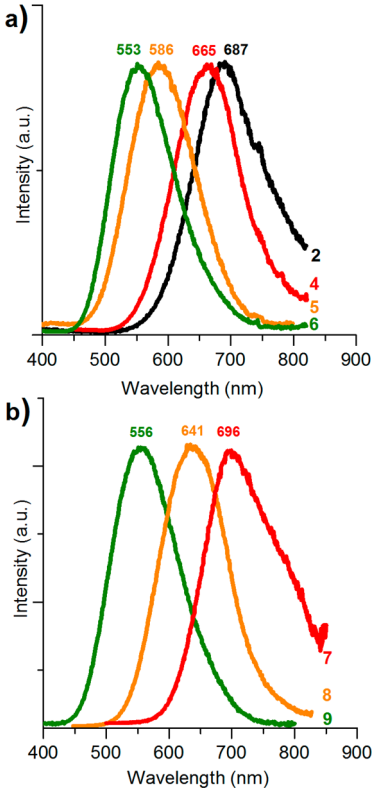

Figure 12. Normalized photoluminescence spectra (λ_{exc} = 375 nm) of quaternary Ag−In−Zn−S nanocrystals dispersions in toluene, batches **2**, **4**, **5**, and **6** (a) and batches **7**, **8**, and **9** (b).

increases with the augmentation of the zinc content, consistent with the modulation of the band gap. The position of the peaks as well as the determined photoluminescence QYs are collected in Table 1. The fwhm values were in the range of 84−127 nm. As expected the QY values are strongly dependent on zinc content, being ca. 50% higher for Zn-rich nanocrystals. The photoluminescence stability should also be underlined, since the measurement of QY was carried out for dispersions stored for one month.

The emission spectra of nanocrystals from batches **7**, **8**, and **9** are presented In Figure 12b. Again, as in the case of series **1**−**6** the maximum of the photoluminescence spectrum hypsochromically shifts with increasing zinc content. The measured fwhm values are in the range of 120−150 nm. The very efficient and stable photoluminescence of nanocrystals from batch **8** should be pointed out. The measured QY after one month of storage was 36.7%—one of the highest values reported for quaternary Ag−In−Zn−S nanocrystals.[21] Higher QYs were only reported for nanocrystals obtained in the above-discussed two-step procedures, involving diffusion-induced phase equilibration through annealing[23,24,27] or for core−shell ternary Ag−In−S/ZnS[62,63] and quaternary Ag−In−Zn−S/ZnS nanocrystals.[64] Concerning the latter case, the deposition of a passivating shell is a known procedure of improving photoluminescence QY in nanocrystals of inorganic semiconductors.[53] This significantly higher photoluminescence QY of core-only nanocrystals was obtained for nanoparticles prepared with the use of increased ratios of indium to silver precursors (from 1/3.4 to 1/5.0). It can therefore be concluded that appropriate contents of indium and zinc in the quaternary nanocrystals are crucial for their photoluminescence.

CONCLUSIONS

To summarize, we elaborated a convenient method of preparation of alloyed quaternary Ag−In−Zn−S nanocrystals in which a multicomponent mixture of simple commercially available precursors is used in ODE solvent. In addition we have shown that the use of auxiliary sulfur precursor (solution of elemental sulfur in OA) in addition to DDT is necessary for the formation of these alloyed nanocrystals; otherwise, ZnS crystals are formed.

By changing the molar ratios of the precursors it is possible to tune the nanocrystal shape (from spheres to rods), size (from 2 to 10 nm in the case of rods), and composition (from 0.75 to 0.24 molar content of $AgInS_2$). The position of their photoluminescence peak can be controllably varied from ca. 550 to ca. 700 nm, with the QY reaching 37% for indium and zinc-rich samples.

ASSOCIATED CONTENT

Supporting Information

Evolution of UV−vis spectra of Ag−In−Zn−S nanocrystals prepared with and without injection of the sulfur solution, X-ray diffractograms and ^{1}H NMR spectra of black solid byproduct, TEM images and histograms of Ag−In−Zn−S nanocrystals (Samples 2, 4, 5, and 6), X-ray diffractograms and EDS spectra of Ag−In−Zn−S nanocrystals prepared under different reaction temperatures (150, 180, and 200 °C). This material is available free of charge via the Internet at http://pubs.acs.org.

AUTHOR INFORMATION

Corresponding Author

*E-mail: piotrbujakchem@poczta.onet.pl. Phone: +48222345584.

Notes

The authors declare no competing financial interest.

ACKNOWLEDGMENTS

This research was carried out in the framework of the project entitled "New solution processable organic and hybrid

(organic/inorganic) functional materials for electronics, optoelectronics and spintronics" (Contract No. TEAM/2011-8/6), which is operated within the Fundation for the Polish Science Team Programme cofinanced by the EU European Regional Development Fund. The TEM images were obtained using the equipment purchased within CePT Project No. POIG.02.02.00-14-024/08-00.

REFERENCES

(1) Murray, C. B.; Norris, D. J.; Bawendi, M. G. *J. Am. Chem. Soc.* **1993**, *115*, 8706−8715.
(2) Peng, Z. A.; Peng, X. *J. Am. Chem. Soc.* **2001**, *123*, 183−184.
(3) Peng, X.; Mann, L.; Yang, W.; Wickham, J.; Scher, E.; Kadavanich, A.; Alivisatos, A. P. *Nature* **2000**, *404*, 59−61.
(4) Bruchez, M., Jr.; Moronne, M.; Gin, P.; Weiss, S.; Alivisatos, A. P. *Science* **1998**, *281*, 2013−2016.
(5) Chan, W. C. W.; Nie, S. *Science* **1998**, *281*, 2016−2018.
(6) Medintz, I. L.; Uyeda, H. T.; Goldman, E. R.; Mattoussi, H. *Nat. Mater.* **2005**, *4*, 435−446.
(7) Kim, S.; Lim, Y. T.; Soltesz, E. G.; De Grand, A. M.; Lee, J.; Nakayama, A.; Parker, J. A.; Mihaljevic, T.; Laurence, R. G.; Dor, D. M.; Cohn, L. H.; Bawendi, M. G.; Frangioni, J. V. *Nat. Biotechnol.* **2004**, *22*, 93−97.
(8) Colvin, V. L.; Schlamp, M. C.; Alivisatos, A. P. *Nature* **1994**, *370*, 354−357.
(9) Coe, S.; Woo, W.-K.; Bawendi, M.; Bulovic, V. *Nature* **2002**, *420*, 800−803.
(10) Tessler, N.; Medvedev, V.; Kazes, M.; Kan, S.; Banin, U. *Science* **2002**, *295*, 1506−1508.
(11) Huynh, W. U.; Dittmer, J. J.; Alivisatos, A. P. *Science* **2002**, *295*, 2425−2427.
(12) McDonald, S. A.; Konstantatos, G.; Zhang, S.; Cyr, P. W.; Klem, E. J. D.; Levina, L.; Sargent, E. H. *Nat. Mater.* **2005**, *4*, 138−142.
(13) Aldakov, D.; Lefrançois, A.; Reiss, P. *J. Mater. Chem. C* **2013**, *1*, 3756−3776.
(14) Scheer, R.; Walter, T.; Schock, H. W.; Fearheiley, M. L.; Lewerenz, H. J. *Appl. Phys. Lett.* **1993**, *63*, 3294−3296.
(15) Guillemoles, J.-F.; Kronik, L.; Cahen, D.; Rau, U.; Jasenek, A.; Schock, H.-W. *J. Phys. Chem. B* **2000**, *104*, 4849−4862.
(16) Kolny-Olesiak, J.; Weller, H. *ACS Appl. Mater. Interfaces* **2013**, *5*, 12221−12237.
(17) Zhong, H.; Bai, Z.; Zou, B. *J. Phys. Chem. Lett.* **2012**, *3*, 3167−3175.
(18) Pan, D.; Weng, D.; Wang, X.; Xiao, Q.; Chen, W.; Xu, C.; Yang, Z.; Lu, Y. *Chem. Commun.* **2009**, 4221−4223.
(19) Zhang, J.; Xie, R.; Yang, W. *Chem. Mater.* **2011**, *23*, 3357−3361.
(20) Torminoto, T.; Adachi, T.; Okazaki, K.; Sakuraoka, M.; Shibayama, T.; Othani, B.; Kudo, A.; Kuwabata, S. *J. Am. Chem. Soc.* **2007**, *129*, 12388−12389.
(21) Yang, X.; Tang, Y.; Tan, S. T.; Bosman, M.; Dong, Z.; Leck, K. S.; Ji, Y.; Demir, H. V.; Sun, X. W. *Small* **2013**, *9*, 2689−2695.
(22) Tang, X.; Yu, K.; Xu, Q.; Choo, E. S. G.; Goh, G. K. L.; Xue, J. *J. Mater. Chem.* **2011**, *21*, 11239−11243.
(23) Tang, X.; Ho, W. B. A.; Xue, J. M. *J. Phys. Chem. C* **2012**, *116*, 9769−9773.
(24) Mao, B.; Chuang, C.-H.; Lu, F.; Sang, L.; Zhu, J.; Burda, C. *J. Phys. Chem. C* **2013**, *117*, 648−656.
(25) Deng, D.; Cao, J.; Qu, L.; Achilefu, S.; Gu, Y. *Phys. Chem. Chem. Phys.* **2013**, *15*, 5078−5083.
(26) Xie, R.; Rutherford, M.; Peng, X. *J. Am. Chem. Soc.* **2009**, *131*, 5691−5697.
(27) Hong, S. P.; Park, H. K.; Oh, J. H.; Yang, H.; Do, Y. R. *J. Mater. Chem.* **2012**, *22*, 18939−18949.
(28) Velapoldi, R. A. *Proc. Conf. NBS Gaithesburg;* National Bureau of Standards: Washington, DC, 1972; Vol. *378*, p 231.
(29) Guo, Q.; Hillhouse, H. W.; Agrawal, R. *J. Am. Chem. Soc.* **2009**, *131*, 11672−11673.
(30) Riha, S. C.; Parkinson, B. A.; Prieto, A. L. *J. Am. Chem. Soc.* **2009**, *131*, 12054−12055.
(31) Steinhagen, C.; Panthani, M. G.; Akhavan, V.; Goodfellow, B.; Koo, B.; Korgel, B. A. *J. Am. Chem. Soc.* **2009**, *131*, 12554−1255.
(32) Kuzuya, T.; Tai, Y.; Yamamuro, S.; Hihara, T.; Peng, D. L.; Sumiyama. *Mater. Trans.* **2004**, *45*, 2650−2652.
(33) Peng, Z. A.; Peng, X. *J. Am. Chem. Soc.* **2002**, *124*, 3343−3353.
(34) Yin, Y.; Alivisatos, P. *Nature* **2005**, *437*, 664−670.
(35) Thomson, J. W.; Nagashima; Macdonald, P. M.; Ozin, G. A. *J. Am. Chem. Soc.* **2011**, *133*, 5036−5041.
(36) Ogawa, T.; Kuzuya, T.; Hamanaka, Y.; Sumiyama, K. *J. Mater. Chem.* **2010**, *20*, 2226−2231.
(37) Chen, B.; Zhong, H.; Zhang, W.; Tan, Z.; Li, Y.; Yu, C.; Zhai, T.; Bando, Y.; Yang, S.; Zou, B. S. *Adv. Funct. Mater.* **2012**, *22*, 2081−2088.
(38) Kim, Y.-K.; Ahn, S.-H.; Chung, K.; Cho, Y.-S.; Choi, C.-J. *J. Mater. Chem.* **2012**, *22*, 1516−1520.
(39) Dai, M.; Ogawa, S.; Kameyama, T.; Okazaki, K.; Kudo, A.; Kuwabata, S.; Tsuboi, Y.; Torimoto, T. *J. Mater. Chem.* **2012**, *22*, 12851−12858.
(40) *Powder Diffraction File, No. 251330;* The JCPDS International Centre for Diffraction Data: Swarthmore, PA, 1990.
(41) *Powder Diffraction File, No. 50566;* The JCPDS International Centre for Diffraction Data: Swarthmore, PA, 1990.
(42) Ogawa, T.; Kuzuya, T.; Hamanaka, Y.; Sumiyama, K. *J. Mater. Chem.* **2010**, *20*, 2226−2231.
(43) Mudryi, A. V.; Victorov, I. A.; Gremenok, V. F.; Patuk, A. I.; Shakin, I. A.; Yakushev, M. V. *Thin Solid Films* **2003**, *431*, 197−199.
(44) Mehdid, M. A.; Djafri, A.; Roussel, C.; Andreoli, F. *Molecules* **2009**, *14*, 4634−4643.
(45) Iwasaki, T.; Higashikawa, K.; Reddy, V. P.; Ho, W. W. S.; Fujimoto, Y.; Fukase, K.; Terao, J.; Kuniyasu, H.; Kambe, N. *Chem.—Eur. J.* **2013**, *19*, 2956−2960.
(46) Pons, T.; Uyeda, H. T.; Medintz, I. L.; Mattoussi, H. *J. Phys. Chem. B* **2006**, *110*, 20308−20316.
(47) Benoit, H.; Doty, P. *J. Phys. Chem.* **1953**, *57*, 958−963.
(48) Cros-Gagneux, A.; Delpech, F.; Nayral, C.; Cornejo, A.; Coppel, Y.; Chaudret. *J. Am. Chem. Soc.* **2010**, *132*, 18147−18157.
(49) Virieux, H.; Le Troedec, M.; Cros-Gagneux, A.; Ojo, W.-S.; Delpech, F.; Nayral, C.; Martinez, H.; Chaudret, B. *J. Am. Chem. Soc.* **2012**, *134*, 19701−19708.
(50) Gabka, G.; Leniarska, K.; Ostrowski, A.; Malinowska, K.; Skorka, L.; Donten, M.; Bujak, P. *Synth. Met.* **2014**, *187*, 94−101.
(51) Kim, D.; Nabeshima, A.; Nakayama, M. *Jpn. J. Appl. Phys.* **2005**, *44*, 1514−1517.
(52) Mesri, D.; Dridi, Z.; Tadjer, A. *Comput. Mater. Sci.* **2007**, *39*, 453.
(53) Protière, M.; Reiss, P. *Small* **2007**, *3*, 399−403.
(54) Pan, D.; Wang, X.; Zhou, Z. H.; Chen, W.; Xu, C.; Lu, Y. *Chem. Mater.* **2009**, *21*, 2489−2493.
(55) Corrado, C.; Jiang, Y.; Oba, F.; Kozina, M.; Bridges, F.; Zhang, J. Z. *J. Phys. Chem. A* **2009**, *113*, 3830−3839.
(56) Hamanaka, Y.; Ogawa, T.; Tsuzuki, M. *J. Phys. Chem. C* **2011**, *115*, 1786−1792.
(57) Zhong, H.; Zhou, Y.; Ye, M.; He, Y.; Ye, J.; He, C.; Yang, C.; Li, Y. *Chem. Mater.* **2008**, *20*, 6434−6443.
(58) Nam, D.-E.; Song, W.-S.; Yang, H. *J. Colloid Interface Sci.* **2011**, *361*, 491−496.
(59) Nam, D.-E.; Song, W.-S.; Yang, H. *J. Mater. Chem.* **2011**, *21*, 18220−18226.
(60) Li, L.; Daou, T. J.; Texier, I.; Chi, T. T. K.; Liem, N. Q.; Reiss, P. *Chem. Mater.* **2009**, *21*, 2422−2429.
(61) Castro, S. L.; Bailey, S. G.; Raffaelle, R. P.; Banger, K. K.; Hepp, A. F. *J. Phys. Chem. B* **2004**, *108*, 12429−12435.
(62) Dai, M.; Ogawa, S.; Kameyama, T.; Okazaki, K.; Kudo, A.; Kuwabata, S.; Tsuboi, Y.; Torimoto, T. *J. Mater. Chem.* **2012**, *22*, 12851−12858.
(63) Chang, J.-Y.; Wang, G.-Q.; Cheng, C.-Y.; Lin, W.-X.; Hsu, J.-C. *J. Mater. Chem.* **2012**, *22*, 10609−10618.

(64) Torimoto, T.; Ogawa, S.; Adachi, T.; Kameyama, T.; Okazaki, K.; Shibayama, T.; Kudo, A.; Kuwabata, S. *Chem. Commun.* **2010**, *46*, 2082−2084.